AIAA JOURNAL
Vol. 34, No. 10, October 1996

Accurate Development of Leading-Edge Vortex Using an Embedded Conical Grid

Anand Kumar*
National Aerospace Laboratories, Bangalore 560017, India

The vortex formation and its development near the apex of a sharp-edged delta wing are poorly represented on conventional grids because of dissimilar length scales of the flow and the grid. The problem is overcome by having an embedded conical grid surrounding the wing. Computed Euler solutions on such an embedded conical grid and on a conventional H-O grid are presented for a range of incidence for a subsonic freestream. The solutions on the embedded conical grid show that the vortex is well resolved right from the apex, even at a very low incidence. The vortex breakdown is well predicted on the embedded conical grid, including the case where the breakdown has just moved upstream of the trailing edge.

Nomenclature

C_p	= pressure coefficient
C_{pt}	= total pressure coefficient
C_{pv}	= pressure coefficient on the vortex axis
C_{pw}	= surface pressure coefficient below the vortex axis
q	= axial velocity
q_v	= axial velocity on the vortex axis
q_∞	= freestream velocity
s	= local semispan
u, v, w	= velocity components
x, y, z	= Cartesian coordinates along the chordwise, wing-normal, and spanwise directions, with the origin at the wing apex
α	= angle of attack
Λ	= wing-sweep angle
ξ, η, ζ	= computational coordinates
Ω_x	= chordwise vorticity
Ω_{xv}	= chordwise vorticity on the vortex axis

Introduction

FLOW over a delta wing at high angles of attack is dominated by flow separating from the leading edges of the wing and forming a pair of counter-rotating vortices, known as the leading-edge or primary vortices, on the lee side of the wing. The lee surface outboard flow, induced by the primary vortices, can separate as it approaches the leading edge to form the secondary vortices. The secondary vortex tends to move the primary vortex inboard and upward from the wing surface. In a similar way, the secondary vortices can give rise to tertiary vortices. The vortex system above the wing plays a very important role in the high-angle aerodynamics of fighter aircraft and missile configurations. The vortex-induced suction generates additional forces that are exploited for maneuverability. Depending on the angle of attack, a sudden change of leading-edge vortex structure, known as the vortex breakdown or burst, can occur above the wing, causing a loss of vortex-induced suction. This severely affects the forces and pitching moment and may limit the useful role of the leading-edge vortex.

Numerical simulations of vortex flow over delta wings employing both Euler equations and Navier–Stokes equations have been carried out.[1–10] Numerical schemes currently employed include central difference type schemes with added artificial dissipation[1–4] and flux splitting[5–7] and flux difference splitting-type upwind schemes.[8–10] Navier–Stokes simulation is needed to resolve the primary separation from the round leading edge and the secondary/tertiary separation on the lee surface. However, to exploit the full potential of the Navier–Stokes simulation the free shear layer and the vortex core should also be resolved. Vortex breakdowns at high incidences are known to be captured in both the Euler and Navier–Stokes computations.

Various types of grid topology, such as O-O, C-O, H-O, C-H, or H-H, are employed for computation of the flow on a delta wing. The O-O grid has the most number of grid points near the wing surface compared with the total number of grid points. A C- or H-type topology in the chordwise direction provides a good description of the wake. An advantage of the H-type topology is that a quasi-three-dimensional grid generation scheme can be used. The present-day codes can handle a more complex grid topology with considerable ease because of the multiblock strategy employed.

The near-apex vortex flow is poorly resolved on conventional grids. A poor vortex resolution leads to a lower suction in the vortex core, and the peak suction in the core gets established well downstream of the apex. Although numerous research papers have been devoted to the numerical simulation of vortex flow over sharp-edged delta wings, the near-apex vortex resolution and its effect on the vortex related phenomena have not been looked into by earlier investigators. The onset and progression of vortex breakdown over the wing, whose consequence is of great importance, may depend on how well the vortex is captured in the flow upstream of the breakdown. Asymmetric breakdown and shock–vortex interaction are some other examples of vortex-related phenomena.

We examine some of the earlier calculations to assess the near-apex vortex resolution. In the $160 \times 32 \times 32$ C-H grid solution given by Hitzel et al.[11] for flow over a 65-deg sharp-edged cropped delta wing at M_∞ of 0.4 and α of 10 deg, a part-span vortex can be inferred from the surface pressure contours, whereas the experiment[12] shows a vortex all along the leading edge. A poor near-apex flow resolution inhibits the vortex formation at this moderate incidence and results in an attached flow. Later, on a $132 \times 32 \times 64$ H-O grid, Hitzel[2] reported a vortex starting from the apex, but the near-apex vortex structure is difficult to assess from the given results. In the $124 \times 36 \times 64$ O-O grid solution reported by Rizzi et al.[13] for the 65-deg wing at α of 10 deg and in the 450×10^3 H-H grid solution reported by Longo[14] for a 60-deg wing at α of 10 deg, the maximum vortex suction in the surface pressure contours occurs downstream of the midchord, which would imply that the near-apex vortex is poorly resolved. A poor near-apex vortex resolution can also be inferred in the $60 \times 64 \times 88$ H-O grid solution of Agrawal et al.[8] for a 70-deg delta wing at α of 30 deg, in the 1600×10^3 H-H grid solution of Webster and Shang[15] for a 70-deg delta wing at α of 33 deg, and in the 2195×10^3 H-H grid solution of Visbal[16] for a 75-deg delta wing in pitching motion, as the peak suction along the vortex axis is established well downstream of the apex. We thus see that the near-apex vortex flow is poorly resolved even when a very fine grid is used.

Received Oct. 4, 1995; revision received Feb. 12, 1996; accepted for publication Feb. 12, 1996.

*Scientist, Computational and Theoretical Fluid Dynamics Division; currently Scientist, Centre for Mathematical Modelling and Computer Simulation, Belur Campus, Bangalore 560037, India.

An aspect of choosing a grid system for the numerical simulation of the flow is whether the grid system is compatible with the flow length scales so that the relevant flow features can be resolved. The transverse dimensions of the vortex near the apex of a sharp-edged delta wing scale with the local semispan of the wing. This can be seen, for example, from the experimental measurements.[17,18] Therefore, a typical transverse length scale of the vortex goes to zero as the apex is approached. The transverse dimensions of the cells of a conventional grid, however, do not diminish as the apex is approached, and hence they become large in comparison to the transverse dimensions of the vortex. Therefore, a conventional grid cannot resolve the near-apex vortex. A grid refinement cannot overcome this inherent deficiency.

The near-apex vortex structure on conventional grids may also suffer from the lack of chordwise grid resolution. Assuming the near-apex flow to be conical, the flow gradients will be large along all of the three coordinates of a conventional grid, thus also requiring a chordwise grid clustering, which is usually not carried out.

To get a better near-apex vortex resolution, both the transverse dimensions of the grid should scale with those of the vortex. Such a grid can be constructed by first laying a block of conical grid surrounding the wing that is then covered by an outer block of a conventional grid. The conical grid may extend in the wing-normal direction as far as to cover the primary vortex region. Since in such a multiblock grid, referred to here as the embedded conical (EC) grid, the transverse dimensions of the near-wing (the vortex region) grid cells scale with those of the vortex as the apex is approached, the grid will have a structure suitable for resolving the near-apex flow, and the grid structure in the aft part of the wing and in the wake will be similar to that of a conventional grid. An earlier study[19] indicated that the vortex is better formed on an EC grid than on a conventional H-O grid.

In the present paper an EC grid is employed to investigate vortex flow over a sharp-edged delta wing. Particular attention is paid to the near-apex vortex structure and its subsequent development. Detailed comparisons of the results with those on a conventional H-O grid are presented. The effect of the near-apex vortex resolution on the vortex breakdown is investigated. The near-apex flow for a very low incidence is presented to examine the potential of the EC grid. Effect of grid refinement is also considered. Computations reported here are based on the Euler equations, which are believed to model the essential features of the sharp-edged delta wing flow, including the breakdown.[2,8,20–22]

Computation of flow over pointed bodies, such as missiles and forebodies, using conventional grids, is also likely to suffer from the lack of grid resolution near the apex. An EC grid can be employed to alleviate the problem.

EC Grid

An EC grid consists of an inner block of conical grid surrounding the wing that is covered by an outer block of a conventional grid. An H-O or a C-O grid topology is a natural choice for the outer block, shown schematically in Fig. 1, but other grid topologies can also be used. The EC grid considered here has an H-O grid as the outer grid. The layout of the grid blocks is shown in Fig. 2, where the boundary conditions on the block faces are also shown.

Let x, y, and z be the Cartesian coordinates along the root chord, wing-normal, and spanwise directions, respectively, with the origin located at the apex, and ξ, η, and ζ be the computational coordinates. A quasi-three-dimensional method is used to generate the grid. The method consists of a plane-by-plane grid generation on ξ planes,

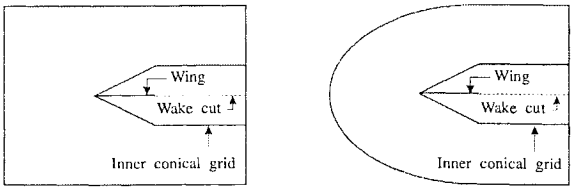

EC grid with an outer H-O grid EC grid with an outer C-O grid

Fig. 1 Schematic of EC grids in the symmetry plane.

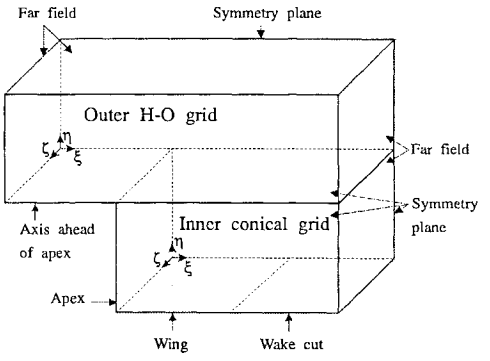

Fig. 2 Layout of the EC grid blocks.

which are taken to be the planes of constant x. In a ξ plane the Laplace equation is used to generate an O-type grid, which is then reclustered in the η direction to give the desired grid. Suitable clusterings are chosen for the apex and the trailing-edge ξ planes, and a linear interpolation between them provides the clustering function for intermediate ξ planes. In the clustering chosen at the apex a specified number of points in the η direction are collapsed onto the apex point to get the inner conical grid. Grids on the ξ planes ahead of the apex are translations of the grid on the apex ξ plane, and similarly grids on the ξ planes downstream of the trailing edge are translations of the grid on the trailing edge ξ plane. Note that the EC grid generation requires the same effort as the H-O grid generation.

Euler Method

The method of Jameson et al.[23] is followed to solve the three-dimensional Euler equations. A cell-centered finite volume scheme is used for spatial discretization. It has second-order spatial accuracy on a uniform grid. An artificial dissipation term consisting of a blend of a second-order term and a fourth-order term is explicitly added to capture shocks and to damp high-frequency spurious numerical oscillations. The artificial dissipation term proposed by Martinelli,[24] suited for highly stretched grids, is used here. The far-field boundary condition is based on one-dimensional Riemann invariants, and a linear extrapolation gives the surface pressure. A five-stage Runge–Kutta scheme with three evaluations of the dissipation term is used for time integration. Local time stepping, implicit residual averaging, and enthalpy damping are employed to accelerate the convergence to steady state. A multiblock scheme is followed. The details of the code can be found in Ref. 25, where an application of the code to the vortex flow over a delta wing is presented and the results compared with the experiment.

Results and Discussion

We consider flow around the sharp-edged delta wing of aspect ratio 1.6 (Λ = 68.2 deg) of Ref. 26. The wing has a flat upper surface, and its maximum thickness is 0.022. The linear dimensions are scaled by the root chord and the velocities by the freestream velocity. The EC grid employed consists of a 60 × 24 × 64 inner conical grid and a 68 × 40 × 64 outer H-O grid. Figure 3 shows a view of the EC grid alongwith views of the inner conical grid and the outer H-O grid. Grids on four ξ planes, scaled by the local semispan, are shown in Fig. 4. Because of the inner conical grid, the near-wing grid quality remains good for the vortex resolution, even close to the apex. The abrupt change in the cell height across the block boundary seen near the apex diminishes very rapidly as one moves away from the apex. A 68 × 64 × 64 conventional H-O grid is also employed. The wing-normal dimension of the grid cell at the apex is 1.8897×10^{-5}. The x coordinates of the ξ planes are the same in both the grids. The number of cells in the EC grid and in the H-O grid are 266,240 and 278,528, respectively. The computational effort to obtain the Euler solutions on the two grids will therefore be comparable.

Results for M_∞ of 0.3 and at several incidences are presented next to highlight the vortex formation near the apex and its development.

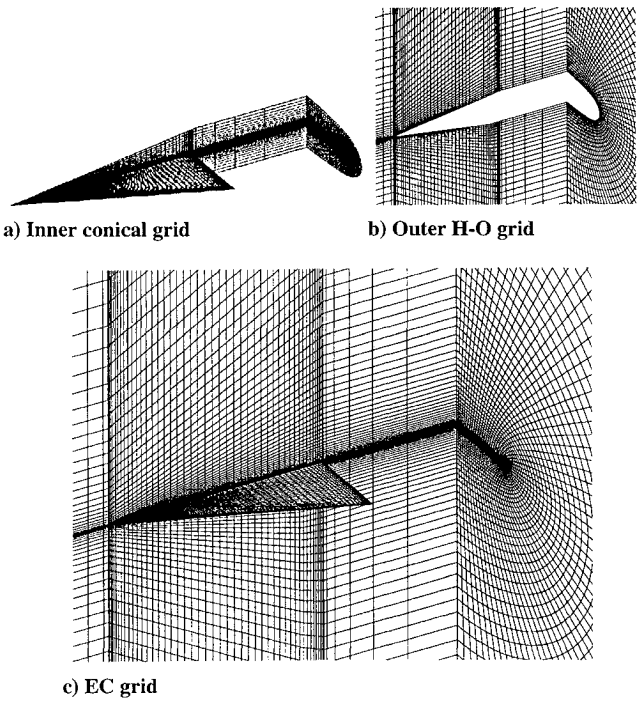

a) Inner conical grid b) Outer H-O grid

c) EC grid

Fig. 3 View of the inner conical grid, the outer H-O grid, and the EC grid.

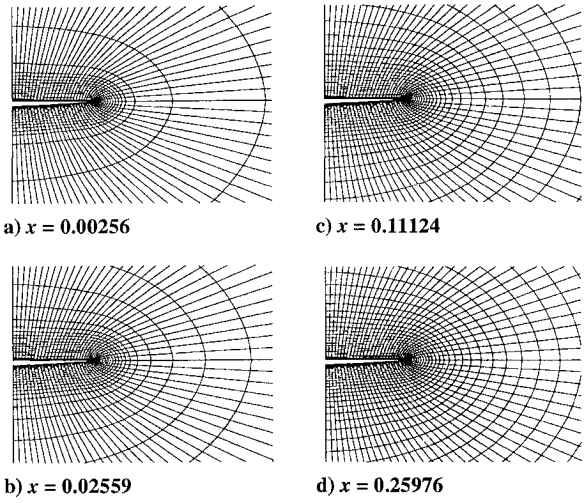

a) $x = 0.00256$ c) $x = 0.11124$

b) $x = 0.02559$ d) $x = 0.25976$

Fig. 4 View of transverse plane grids in the apex region.

Flow at 10-deg Incidence

Figure 5 shows the velocity vectors and contours of q, C_p, and Ω_x for α of 10 deg given by the EC solution on the first transverse cell plane (TCP) (the TCPs are the x planes passing through the cell centers and are numbered in the downstream direction, starting from the apex), $x = 0.00128$, and by the H-O solution on the fifth TCP, $x = 0.02158$. The vortex center in a TCP is the point of maximum total pressure loss, and the line joining the vortex centers is the vortex axis. Axial velocity is the velocity along the mean vortex axis that is defined to be the line joining the apex to the vortex center. The velocity vectors show flow separating at the leading edge and forming a vortex above the wing in both the solutions. The EC solution q contours show a well-resolved jet-like pattern, and the maximum of q is significantly higher than q_∞, whereas the H-O solution q contours do not show the jet-like pattern of the vortex even on the fifth TCP. (The reason for not showing the H-O solution on the first TCP is apparent.) There are only five cells between the wing and the vortex center at this TCP in the H-O solution compared with 18 cells at the first TCP in the EC solution, and hence a better resolved vortex structure in the EC solution. The C_p and Ω_x contours also show the striking difference in their resolution on the two grids.

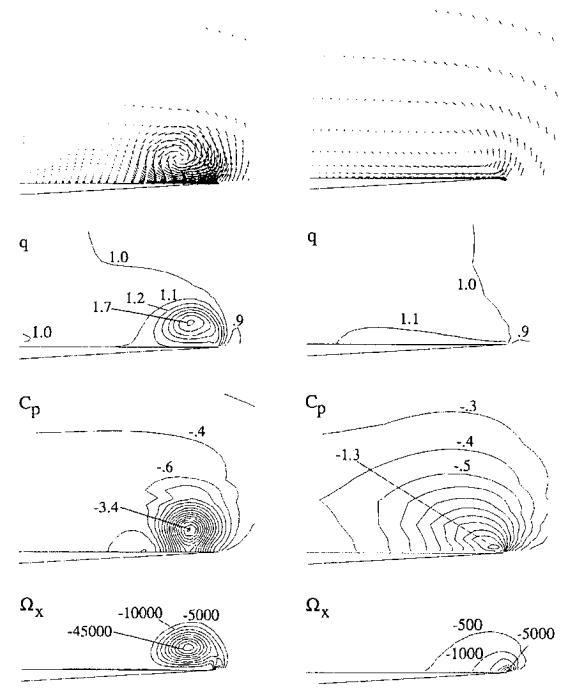

EC grid, $x = 0.00128$ H-O grid, $x = 0.02158$

Fig. 5 Crossflow velocity vectors and contours of q, C_p, and Ω_x near the apex ($\alpha = 10$ deg).

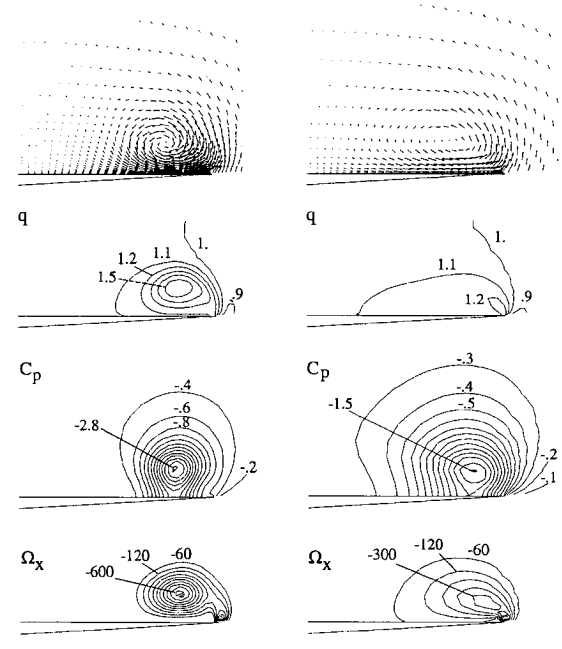

EC grid H-O grid

Fig. 6 Crossflow velocity vectors and contours of q, C_p, and Ω_x ($\alpha = 10$ deg and $x = 0.1$).

Figure 6 shows velocity vectors and contours of q, C_p, and Ω_x at $x = 0.1$ (11th TCP). The vortex in the H-O solution, as seen from the q contours, is poorly resolved. There are 18 cells between the wing and the vortex center in the EC solution, which is the same as that at the first TCP, showing a uniform resolution of the apex region flow. There are eight cells between the wing and the vortex center in the H-O solution at $x = 0.1$. The number of cells between the wing and the vortex center diminishes in the H-O solution as the apex is approached. This is precisely the reason why the near-apex vortex resolution on an H-O grid (or any other conventional grid) will be poor. The H-O solution is seen to give lower values of $-C_p$ and $-\Omega_x$ in the vortex core. These contours are better formed as compared with those at $x = 0.02158$ (Fig. 5), which shows that as

we move downstream the vortex develops and the flow features do improve, as expected. We also observe that the pressure field in the H-O solution is better formed than the velocity field.

Figure 7 compares distribution of q_v, C_{pv}, Ω_{xv}, and C_{pw}. Since Ω_{xv} behaves as s^{-1} near the apex, $\Omega_{xv}s$ is plotted. The vortex development in the two solutions differs considerably. The quantities q_v, $-C_{pv}$, $-\Omega_{xv}s$, and $-C_{pw}$ are quickly established in the EC solution and thereafter have a monotonic decreasing trend. In the H-O solution, they are much lower initially and increase as the vortex develops and then decrease. These quantities at $x = 0.1$ in the H-O solution differ from those in the EC solution by 26, 47, 53, and 31%, and at $x = 0.3$ by 14, 28, 30, and 18%, respectively. The values of C_{pv}, q_v, and Ω_{xv} at $x = 0.1$ are given in Table 1. The maximum of $-C_{pv}$ in the EC solution is 3.453 and occurs at the first TCP, whereas its value in the H-O solution is 1.819 and occurs at $x = 0.418$ (Table 2). Thus, the H-O solution vortex develops to its peak suction well downstream of the apex. The maximum of $-C_{pw}$ in the H-O solution occurs at $x = 0.31$. The H-O solution surface C_p contours will therefore show the peak suction to be at $x = 0.31$. Such a feature in the surface C_p contours can be used to infer that the peak suction on the vortex axis is attained well downstream of the apex.

Figure 8 compares C_p across the vortex core (on the line passing through the vortex center and parallel to the wing) and on the wing at $x = 0.1, 0.3, 0.5$, and 0.7. The conical nature of the flow is clearly seen in the EC solution. The EC solution vortex core shows higher gradients and consequently higher suction. The H-O solution vortex core is seen to be much broader near the apex because of its poor resolution. The EC solution C_p profiles show a monotonic behavior along x, whereas the H-O solution C_p profiles show that peak suction in the core and on the wing are attained well downstream of the apex.

Flow at 20-deg Incidence

Figure 9 compares distributions of q_v, $-C_{pv}$, $-\Omega_{xv}s$, and $-C_{pw}$ given by the two solutions at α of 20 deg. The peak values of these quantities are seen to be quickly established for the EC solution and decrease monotonically until vortex breakdown. The maximum of q_v is more than two times q_∞. The maximum of $-C_{pv}$ is 6.352 and occurs at $x = 0.0329$. These quantities in the H-O solution are considerably lower near the apex. Their values in the H-O solution at $x = 0.1$ differ from those in EC solution by 21, 27, 45, and 7%, respectively. As the vortex develops, q_v, $-C_{pv}$, and $-\Omega_{xv}s$ increase and, unlike the 10-deg case, become larger than those in the EC solution before decreasing. The maximum of $-C_{pv}$ in the H-O solution is 4.837 and occurs at $x = 0.3339$. The maximum of $-C_{pv}$ at α of 10 deg occurs at $x = 0.418$, which may show that as the vortex becomes stronger it lies higher above the wing, will have more cells in the η direction for its resolution, and therefore may take a shorter axial length to develop to its peak suction. As the vortex is located higher (cf. the 10-deg case), the C_{pw} in the two solutions differ much less compared with C_{pv}, and the maximum of $-C_{pw}$ in the H-O solution occurs closer to the apex.

Table 1 C_{pv}, q_v, and Ω_{xv} at $x = 0.1$

	EC grid			H-O grid		
α, deg	C_{pv}	q_v	Ω_{xv}	C_{pv}	q_v	Ω_{xv}
10	−2.860	1.584	−647.7	−1.510	1.161	−302.0
20	−5.969	2.069	−715.6	−4.315	1.632	−392.8
25	−8.032	2.385	−811.5	−6.053	1.895	−464.8
30	−9.871	2.875	−940.3	−7.876	2.236	−556.2

Table 2 Minimum of C_{pv} and its x location

	EC grid		H-O grid	
α, deg	$C_{pv_{\min}}$	$x_{C_{pv\min}}$	$C_{pv_{\min}}$	$x_{C_{pv\min}}$
10	−3.453	0.00128	−1.819	0.4180
20	−6.352	0.0329	−4.837	0.3339
25	−8.516	0.0301	−6.497	0.2481
30	−10.402	0.0255	−8.169	0.2135

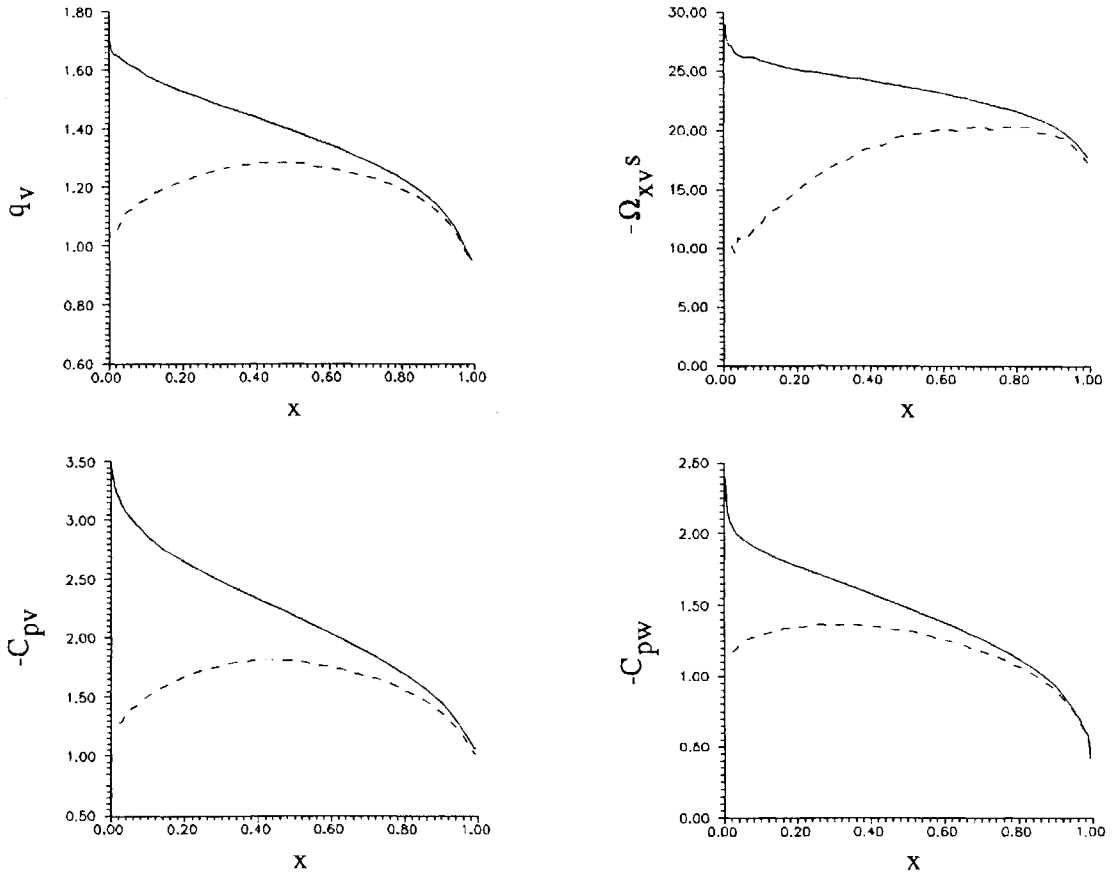

Fig. 7 Comparisons of q_v, C_{pv}, $\Omega_{xv}s$, and C_{pw} on the two grids (α = 10 deg): ——, EC grid and - - - -, H-O grid.

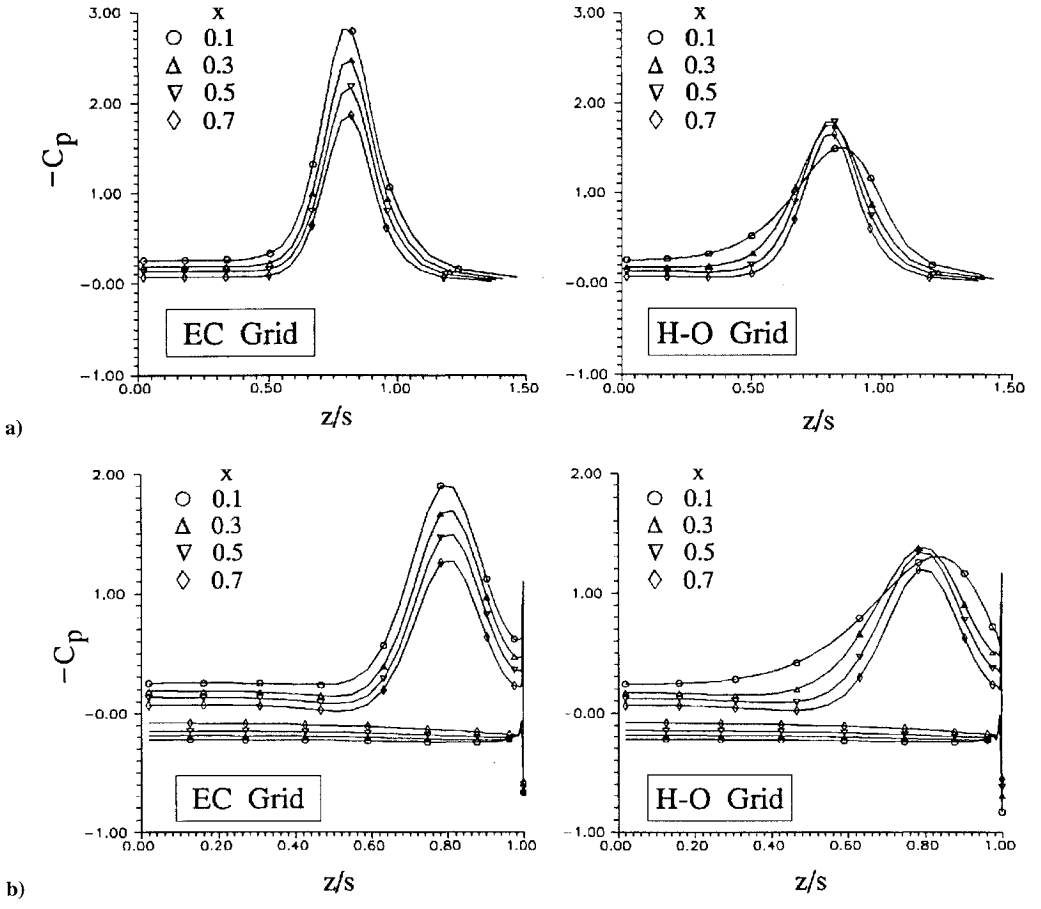

Fig. 8 Pressure distribution a) across the vortex core and b) on the wing (α = 10 deg).

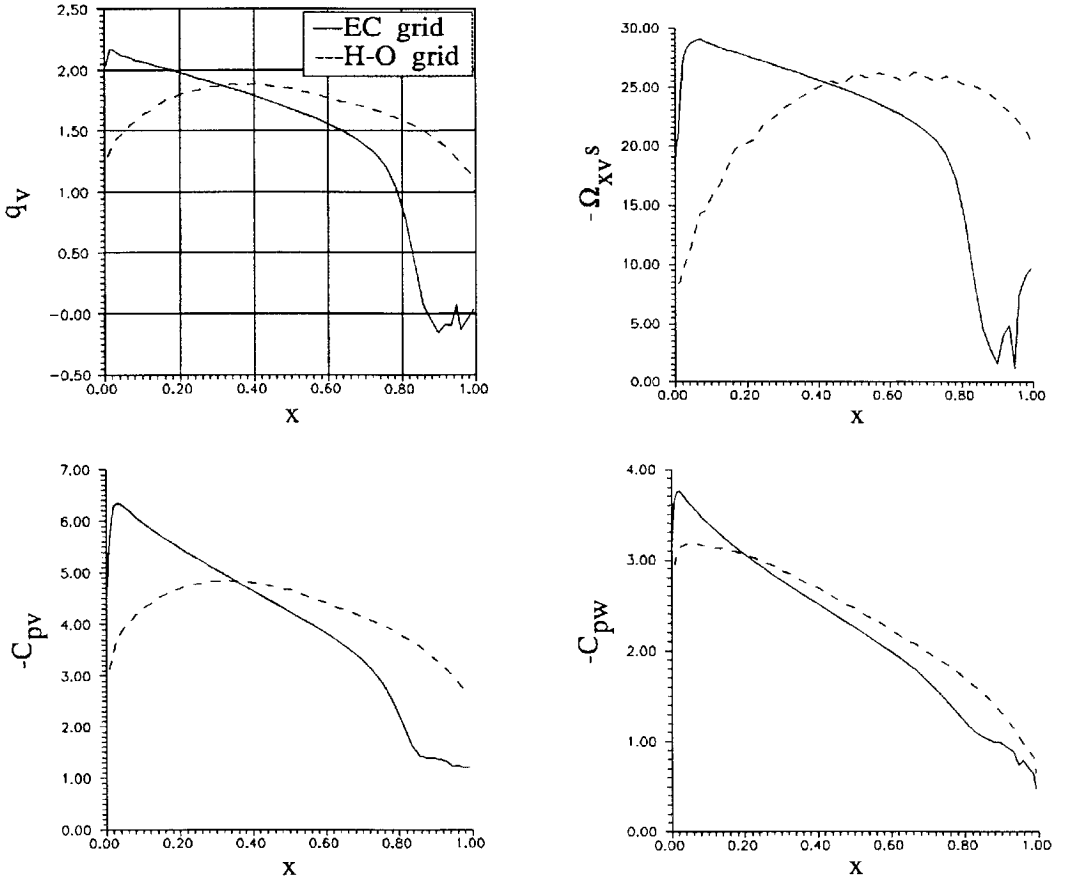

Fig. 9 Comparisons of q_v, C_{pv}, $\Omega_{xv}s$, and C_{pw} on the two grids (α = 20 deg).

The EC solution as a result of vortex breakdown shows a rapid decrease in $-C_{pv}$, q_v, and $-\Omega_{xv}s$ downstream of $x = 0.75$. The flow on the vortex axis is observed to reverse at $x = 0.87$. The breakdown predicted on the EC grid is consistent with the experimental observation.[26] Vortex breakdown, however, is not observed in the H-O solution. In a situation like flow over a delta wing, the vortex breakdown phenomenon involves a complex interaction of the pressure and velocity fields in the presence of the wing. The basic concept of criticality[27] may, however, still be applicable, although a simple breakdown criterion, such as one based on the swirl parameter, may not be possible. In the EC solution the vortex gets well established very close to the apex and the axial flow decelerates and appears to reach conditions necessary for the breakdown, towards the trailing edge. The H-O solution vortex gets fully established much downstream of the apex, and although the axial flow decelerates, the flow may not be near the conditions to initiate the breakdown over the wing.

The time integration method employed here is pseudounsteady. Pseudounsteady methods have been employed by several investigators[2,14,20–22] for vortex breakdown investigations. The results presented correspond to a certain time step.

Figure 10 shows velocity vectors and contours of q, C_p, and Ω_x given by the two solutions at $x = 0.1$. There are 21 cells between the wing and the vortex center in the EC solution, which is same as that at the first TCP, showing once again a uniform resolution of the apex region flow. There are 10 cells between the wing and the vortex center in the H-O solution compared with six cells at the fifth TCP. The H-O solution q contours show that the vortex is not well formed. The suction and vorticity and their gradients in the core are lower in the H-O solution. Further comparisons of the flowfield given by the two solutions can be found in Ref. 28.

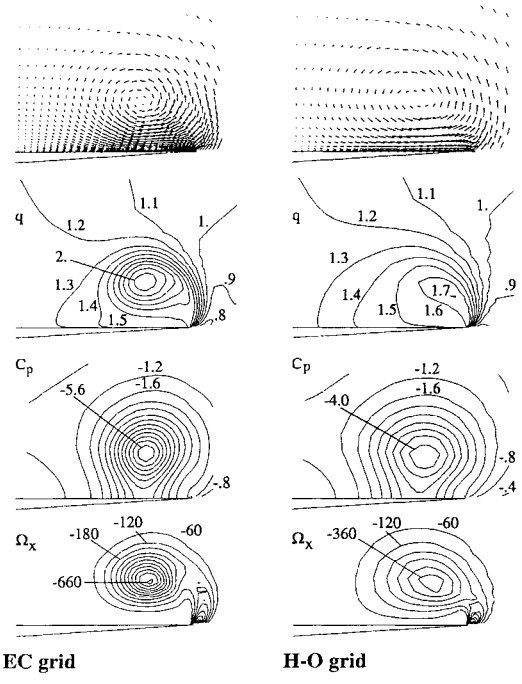

EC grid H-O grid

Fig. 10 Crossflow velocity vectors and contours of q, C_p, and Ω_x (α = 20 deg and x = 0.1).

Flow at 30-deg Incidence

Figure 11 compares distributions of q_v, $-C_{pv}$, $-\Omega_{xv}s$, and $-C_{pw}$ given by the two solutions at α of 30 deg. Peak values of these quantities in the EC solution are established very close to the apex. The maximum of $-C_{pv}$ is 10.402 and occurs at $x = 0.0255$. The maximum of q is about three times q_∞. The quantities q_v, $-C_{pv}$, and $-\Omega_{xv}s$ are considerably lower in the H-O solution over the fore part of the wing, and as the vortex develops, the differences between the two solutions decrease. They differ from those in the EC solution by 22, 20, and 40%, respectively, at $x = 0.1$. The maximum of $-C_{pv}$ in the H-O solution is 8.169 and occurs at $x = 0.2135$. The breakdown location predicted by the H-O solution is fairly close to that given by the EC solution, although the solutions differ considerably in the apex region.

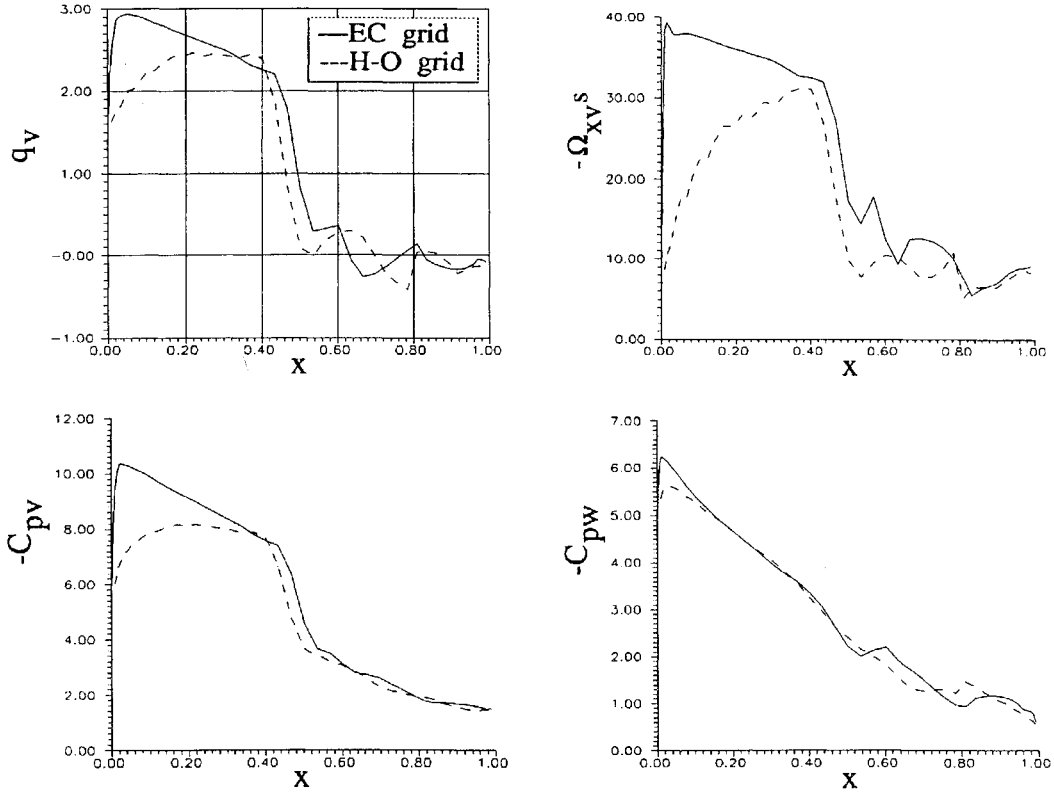

Fig. 11 Comparisons of q_v, C_{pv}, $\Omega_{xv}s$, and C_{pw} on the two grids (α = 30 deg).

The vortex structure for α of 30 deg in the EC solution is also found[29] to be well resolved on the first TCP. Figure 12 shows contours of q, C_p, and Ω_x given by the two solutions at $x = 0.1$. The q contours show that the vortex is still poorly resolved on the H-O grid. The EC solution shows larger q, $-C_p$, and $-\Omega_x$, and higher gradients in the core. Further comparisons of the flowfield given by the two solutions can be found elsewhere.[28,29]

The development of the vortex for various incidences is summarized from the C_{pv} distribution, shown in Fig. 13. The peak suction on the vortex axis in the EC solutions is established very close to the apex for all incidences, whereas in the H-O solutions it is established well downstream of the apex, and its location moves closer to the apex as the incidence increases (Table 2). The vortex structure on the EC grid is uniformly well resolved right from the apex at all incidences. In the H-O solutions, the velocity field near the apex is significantly distorted, although it is seen to improve with the increase in the incidence and as one moves downstream from the apex. The pressure field, however, is less distorted, although the gradients in the core and the maximum suction are lower. Because of a more accurate representation of the vortex structure near the apex and its subsequent development, the vortex breakdown, which involves a complex interaction of the velocity and pressure fields, can be expected to be better represented in the EC solutions. This is seen for the 20-deg case.

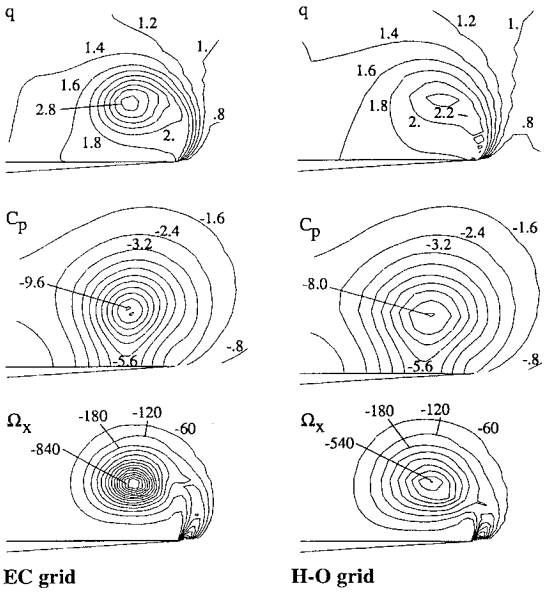

Fig. 12 Contours of q, C_p, and Ω_x (α = 30 deg and x = 0.1).

Flow at 1-deg Incidence

We consider flow at α of 1 deg to demonstrate that the vortex near the apex remains well resolved on the EC grid even at a low incidence. (This can be a good test case for vortex simulation on conventional grids.) Figure 14 shows contours of C_{pt}, u, C_p, and Ω_x on the first TCP. A well-resolved vortex is seen from the C_{pt} contours. The u contours show the jet-like feature of the vortex core. The C_p and Ω_x contours also show that the vortex is well resolved.

Effect of Grid Refinement

We consider grid refinement in the η direction only, since the resolution in this direction is most critical. In addition to the fine EC grid, used earlier, a coarse, a medium, and an ultrafine EC grid are considered. In the η direction, the inner conical grid and the outer H-O grid have 12 and 20 cells, respectively, for the coarse grid, 18 and 30 cells for the medium grid, 24 and 40 cells for the fine grid, and 30 and 50 cells for the ultrafine grid. The coarse grid is obtained by deleting the alternate points along η of the fine grid.

Figure 15 shows q_v, C_{pv}, and C_p across the vortex core and on the wing at $x = 0.1$, obtained on the four EC grids for α of 20 deg. The maximum of $-C_{pv}$ is seen to be established very quickly even on the coarse grid. The C_p across the vortex core shows that the flow outside the subcore converges with grid refinement. The values on the vortex axis, q_v and $-C_{pv}$, are seen to increase with the grid refinement; the increments, however, reduce with successive grid refinement. The grid refinement is seen to have little effect on the outer flow supporting the vortex. The change in the C_p as a result of grid refinement is smaller on the wing than in the core.

Figure 15 also shows that the coarser EC grids do not capture the breakdown, whereas it is captured on the fine EC grid. The

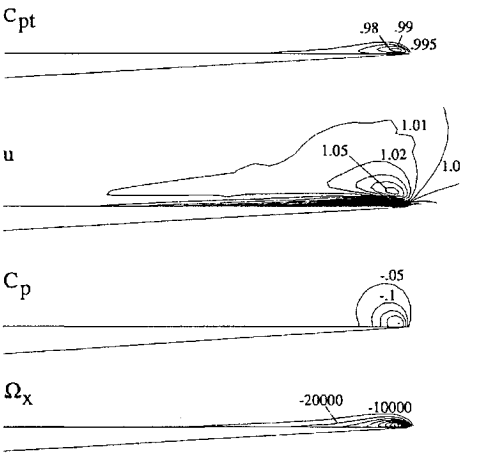

Fig. 14 Contours of C_{pt}, u, C_p, and Ω_x (α = 1 deg and x = 0.00128).

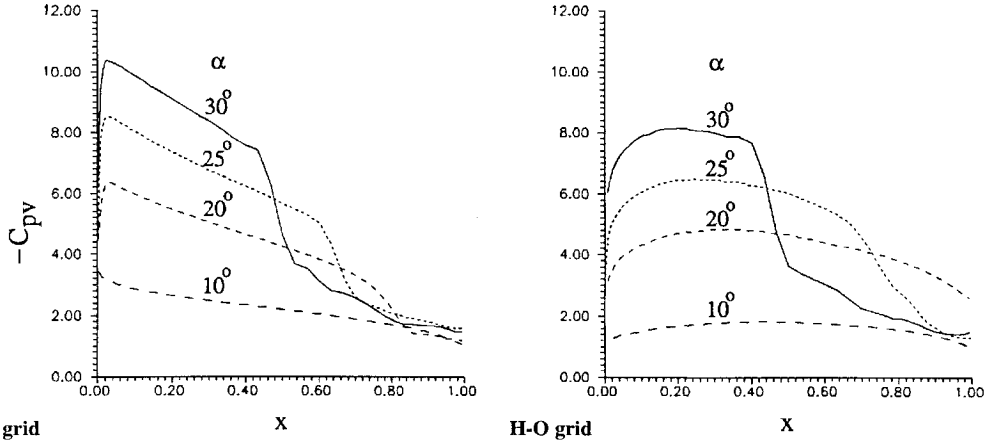

Fig. 13 C_{pv} at different incidences on the two grids.

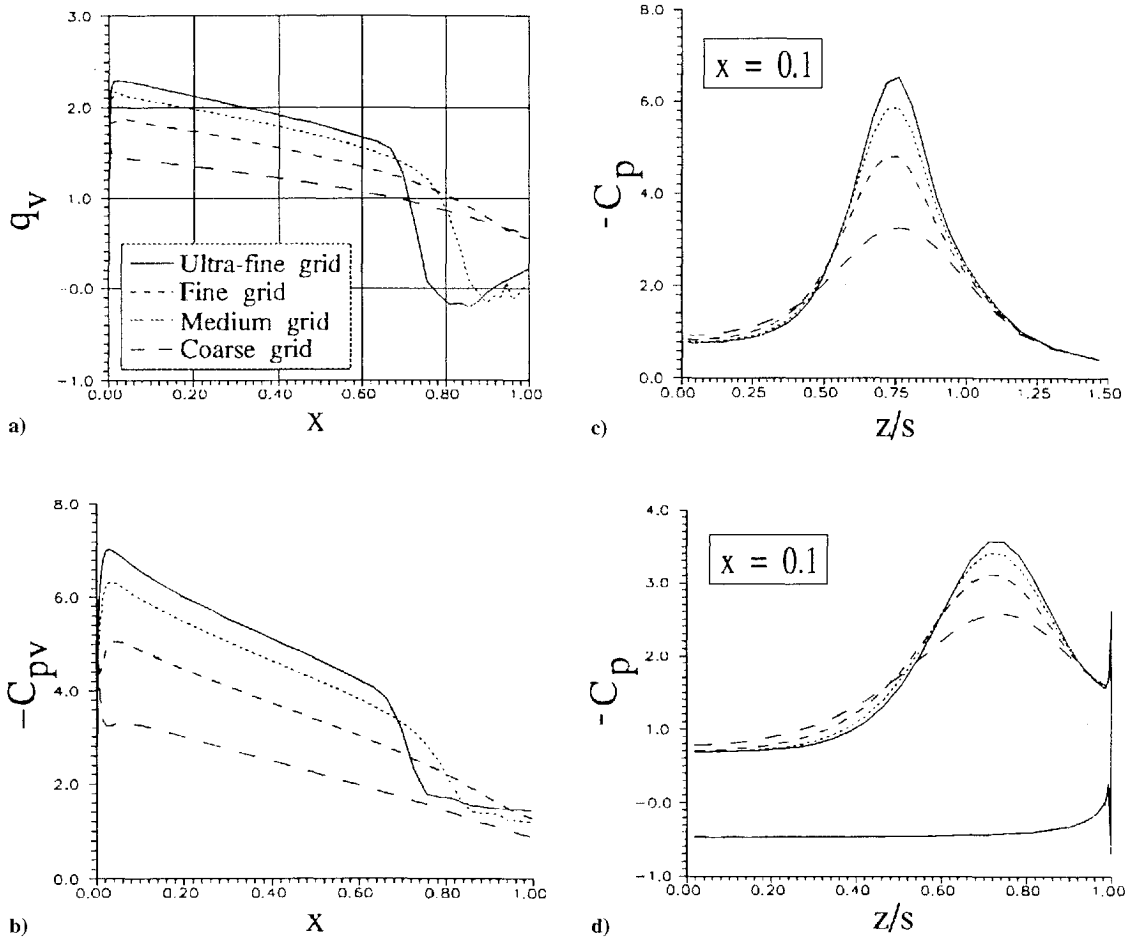

Fig. 15 Effect of grid refinement on a) q_v, b) C_{pv}, c) C_p across the vortex core, and d) C_p on the wing (α = 20 deg).

H-O grid used here does not capture the breakdown for this case (Fig. 9) and may require further refinement. Thus, in comparison to the conventional H-O grid, the EC grid requires fewer grid points for the breakdown to be captured when it is mild (located close to the trailing edge).

Computations reported, except the ultrafine grid computation, have been carried out on a four processor (Intel 860) Flosolver, a parallel computer developed at the National Aerospace Laboratories. A computation consisting of 2000 time steps on the coarse grid and 3000 time steps on the fine grid takes about 80 CPU hours. The ultrafine grid computation has been carried out on the Convex 3820 supercomputer at the Centre for Mathematical Modelling and Computer Simulation, taking about 22 CPU hours.

Conclusions

Numerical investigation of vortex flow on a sharp-edged delta wing of aspect ratio 1.6 is carried out on an embedded conical grid and on a conventional H-O grid. Particular attention is paid to the near-apex vortex structure. On the EC grid, the vortex is found to be well resolved right from the apex for all incidences. Even at a very low incidence, the vortex remains well resolved near the apex. The suction on the vortex axis attains its peak very close to the apex. Velocity and pressure distributions in the vortex core show a conical behavior. These aspects of the vortex flowfield are not satisfactorily resolved on the comparable H-O grid.

Vortex breakdown cases at 20- and 30-deg incidence are considered. The vortex breakdowns in both the cases are well captured on the EC grid. The conventional H-O grid used here, although reasonably fine, does not capture the breakdown at the lower incidence. The more accurate representation of the vortex velocity and pressure fields on the EC grid makes it highly suited for simulation of vortex-related phenomena, such as the vortex breakdown.

Acknowledgments

The author would like to thank Shailendra Prasad for the preparation of the figures. Helpful suggestions by K. S. Yajnik and K. S. Ravichandran are gratefully acknowledged.

References

[1]Rizzi, A., Eriksson, L. E., Schmidt, W., and Hitzel, S. M., "Numerical Solution of the Euler Equations Simulating Vortex Flow Around Wings," *Aerodynamics of Vortical Type Flows in Three Dimensions*, AGARD-CP-342, 1983, pp. 21.1–21.14.

[2]Hitzel, S. M., "Wing Vortex-Flows up into Vortex Breakdown—A Numerical Simulation," *Proceedings of the AIAA 6th Applied Aerodynamics Conference*, AIAA, Washington, DC, 1988, pp. 73–83 (AIAA Paper 88-2518).

[3]Kumar, A., and Das, A., "Computation of Vortex Flow on a Delta Wing at Transonic Speed," *Symposium Transsonicum III*, edited by J. Zierep and H. Oertel, Springer–Verlag, Berlin, 1988, pp. 317–328

[4]Hilgenstock, A., "Validation of Transonic Turbulent Flows Past Delta Wing Configurations," *Aeronautical Journal*, Vol. 95, Aug./Sept. 1991, pp. 219–230.

[5]Fujii, K., and Schiff, L. B., "Numerical Simulation of Vortical Flows over a Strake Delta Wing," AIAA Paper 87-1229, June 1987.

[6]Thomas, J. L., Taylor, S. L., and Anderson, W. K., "Navier–Stokes Computations of Vortical Flows over Low Aspect Ratio Wings," *AIAA Journal*, Vol. 28, No. 2, 1990, pp. 205–212.

[7]Ekaterinaris, J. A., and Schiff, L. B., "Vortical Flows over Delta Wings and Numerical Prediction of Vortex Breakdown," AIAA Paper 90-0102, Jan. 1990.

[8]Agrawal S. A., Barnet, R. M., and Robinson, B. A., "Numerical Investigation of Vortex Breakdown on a Delta Wing," *AIAA Journal*, Vol. 30, No. 3, 1992, pp. 584–591.

[9]Bannink, W. J., and Houtman, E. M., "Experimental and Computational Study of the Vortical Flow over a Delta Wing at High Angles of Attack," *IUTAM Symposium on Fluid Dynamics of High Angles of Attack*, edited by R. Kawamura and Y. Aihara, Springer–Verlag, Berlin, 1992, pp. 399–411.

[10]Kandil, H., Kandil, O., and Liu, C., "Supersonic Vortex Breakdown over a Delta Wing at High Angles of Attack," *Proceedings of the AIAA 11th Applied Aerodynamics Conference*, AIAA, Washington, DC, 1993, pp. 582–596 (AIAA Paper 93-3472).

[11]Hitzel, S. M., Wagner, B., and Leicher, S., "Euler Simulation of the Vortex Flow Experiment—A Critical Consideration," *Proceedings of Symposium on International Vortex Flow Experiment on Euler Code Validation*, edited by A. Elsenaar and G. Eriksson, Aeronautical Research Inst. of Sweden (FFA), Broma, Sweden, 1986, pp. 281–288.

[12]Borsen, S. J., and Elsenaar, A., "Tests on the AFWAL 65° Wing at NLR: A Study of Vortex Flow Development Between Mach = 0.4 and 4," *Proceedings of Symposium on International Vortex Flow Experiment on Euler Code Validation*, edited by A. Elsenaar and G. Eriksson, Aeronautical Research Inst. of Sweden (FFA), Broma, Sweden, 1986, pp. 23–36.

[13]Rizzi, A., Drougge, G., and Purcell C. J., "Euler Simulation of Shed Vortex Flows over the 65 Degree Delta Wings," *Proceedings of Symposium on International Vortex Flow Experiment on Euler Code Validation*, edited by A. Elsenaar and G. Eriksson, Aeronautical Research Inst. of Sweden (FFA), Broma, Sweden, 1986, pp. 289–343.

[14]Longo, J. M. A., "The Compressible Inviscid Vortex Flow on a Sharp Edge Delta Wing," International Council of the Aeronautical Science, ICAS Paper 94-4.3.3, Sept. 1994.

[15]Webster, W. P., and Shang, J. S., "Numerical Simulation of Vortex Breakdown over a Delta Wing," AIAA Paper 91-1814, June 1991.

[16]Visbal, M. R., "Onset of Vortex Breakdown Above a Pitching Delta Wing," *AIAA Journal*, Vol. 32, No. 8, 1994, pp. 1568–1575.

[17]Nelson, R. C., and Visser, K. D., "Breaking Down the Delta Wing Vortex—The Role of Vorticity in the Breakingdown Process," *Vortex Flow Aerodynamics*, AGARD-CP-494, 1990, pp 21.1–21.15.

[18]Earnshaw, P. B., "An Experimental Investigation of the Structure of a Leading-Edge Vortex," Aeronautical Research Council, R&M 3281, March 1961.

[19]Kumar, A., and Sudharsan, R., "Computation of Vortex Flow on a Delta Wing Using a Multi-Block Grid," *Computational Fluid Dynamics Journal*, Vol. 4, No. 1, 1995, pp. 99–112.

[20]Modiano, D. L., and Murman, E. M., "Adaptive Computations of Flow Around a Delta Wing with Vortex Breakdown," *AIAA Journal*, Vol. 32, No. 7, 1994, pp. 1545–1547.

[21]Kumar, A., "Burst Vortex Flow-Field on a Delta Wing—A Numerical Simulation Using Euler Equations," *Current Science*, Vol. 68, No. 3, 1995, pp. 330–333.

[22]Longo, J. M. A., "Simulation of Complex Inviscid and Viscous Vortex Flows," *IUTAM Symposium on Fluid Dynamics of High Angles of Attack*, edited by R. Kawamura and Y. Aihara, Springer–Verlag, Berlin, 1992, pp. 363–373.

[23]Jameson, A., Schmidt, W., and Turkel, E., "Numerical Solution of Euler Equations by Finite Volume Method Using Runge–Kutta Time-Stepping Scheme," AIAA Paper 81-1259, June 1981.

[24]Martinelli, L., "Calculation of Viscous Flows with a Multigrid Method," Ph.D. Thesis, MAE Dept., Princeton Univ., Princeton, NJ, 1987.

[25]Kumar, A., "Navier–Stokes Simulation of Transonic Vortex Flow over a Delta Wing," *Proceedings of Fluid Dynamics Symposium in Honour of Professor R. Narasimha*, National Aerospace Laboratories, SP 9315, Bangalore, India, 1993, pp. 77–89.

[26]Hummel, D., and Srinivasan, P. S., "Vortex Breakdown Effects on the Low-Speed Aerodynamic Characteristics of Slender Delta Wing in Symmetric Flow," *Journal of Royal Aeronautical Society*, Vol. 71, April 1967, pp. 319–322.

[27]Benjamin, T. B., "Theory of Vortex Breakdown Phenomenon," *Journal of Fluid Mechanics*, Vol. 14, Pt. 4, 1962, pp. 593–629.

[28]Kumar, A., "An Embedded Conical Grid for Leading-Edge Vortex Flow Simulation," National Aerospace Laboratories, CF-PD-9518, Bangalore, India, Aug. 1995.

[29]Kumar, A., "Numerical Simulation of Leading-Edge Vortex Breakdown Using Euler Equations," *Proceedings of 1st Asian Computational Fluid Dynamics Conference*, edited by W. H. Hui, Y. K. Kwok, and J. R. Chasnov, Hong Kong Univ. of Science and Technology, Hong Kong, 1995, pp. 513–518.